

Hurwitz, Braesicke and Pyle (2010b)
Future Stratospheric Climate Change
1

1 **Contributors to Future Stratospheric Climate Change: An**
2 **Idealized Chemistry–Climate Model Sensitivity Study**

3

4 **M. M. Hurwitz ^{1,2}, P. Braesicke ¹ and J. A. Pyle ¹**

5

6 **1 Centre for Atmospheric Science and NCAS–Climate, University of**
7 **Cambridge, Cambridge, UK**

8 **2 Now at: NASA Postdoctoral Program, NASA Goddard Space Flight Center,**
9 **Greenbelt, MD, USA**

10

11 Corresponding author information

12 Email address: **margaret.m.hurwitz@nasa.gov**

13

14 Mailing address: **NASA Goddard Space Flight Center**
15 **Code 613.3**
16 **Greenbelt, MD**
17 **USA 20771**

18

18 **Abstract**

19 Within the framework of an idealized model sensitivity study, three of the main
20 contributors to future stratospheric climate change are evaluated: increases in
21 greenhouse gas concentrations, ozone recovery, and changing sea surface
22 temperatures (SSTs). These three contributors are explored in combination and
23 separately, to test the interactions between ozone and climate; the linearity of
24 their contributions to stratospheric climate change is also assessed.

25

26 In a simplified chemistry–climate model, stratospheric global mean temperature
27 is most sensitive to CO₂ doubling, followed by ozone depletion, then by
28 increased SSTs. At polar latitudes, the Northern Hemisphere (NH) stratosphere is
29 more sensitive to changes in CO₂, SSTs and O₃ than is the Southern Hemisphere
30 (SH); the opposing responses to ozone depletion under low or high background
31 CO₂ concentrations, as seen with present–day SSTs, are much weaker and are
32 not statistically significant under enhanced SSTs. Consistent with previous
33 studies, the strength of the Brewer–Dobson circulation is found to increase in an
34 idealized future climate; SSTs contribute most to this increase in the upper
35 troposphere/lower stratosphere (UT/LS) region, while CO₂ and ozone changes
36 contribute most in the stratosphere and mesosphere.

37

37 **1 Motivations**

38 Braesicke et al., 2006; hereafter BHP2006) examined the stratospheric sensitivity
39 to ozone depletion and to the doubling of CO₂. Their study used a sea surface
40 temperature (SST) climatology with a repeating annual cycle, representative of
41 the late 20th century. That is, SSTs did not increase in response to increased
42 greenhouse gas concentrations; their experiments primarily examined the
43 stratospheric radiative impact of increased CO₂.

44

45 Using the same simplified chemistry–climate model (CCM) as in BHP2006, the
46 relative response to changes in CO₂ and O₃ concentrations and sea surface
47 temperatures (SSTs) is explored; this approach considers the combined
48 stratospheric response to warming from both the troposphere and the upper
49 ocean by prescribing ‘future’ SSTs. To separate the three proposed contributions
50 to stratospheric climate change, global mean temperature, eddy heat flux,
51 winds and ozone are diagnosed in each of a set of idealized time–slice
52 experiments. The strength of the Brewer-Dobson circulation, and the
53 connection between tropical upwelling and polar ozone in an idealized
54 present–day climate scenario is compared with an idealized future climate.

55

56 BHP2006 found that global mean temperatures cooled in response to both an
57 O₃ change (2000–like – 1980–like) and a CO₂ change (704ppmv – 352ppmv),
58 throughout the middle atmosphere. However, neither change much affected
59 tropospheric temperatures because the same SST climatology was prescribed in
60 all experiments. Recent trends in observed SSTs, as well as coupled ocean–
61 atmosphere simulations of the 21st century, suggest that anthropogenic climate
62 change will continue to affect the temperature of the sea surface (i.e. Johns et
63 al., 2003). When ‘future’ SSTs are used in conjunction with a doubled–CO₂
64 atmosphere, the troposphere should respond by warming more significantly
65 than for a doubling of CO₂ alone. Also, there may be feedbacks between

66 these increased tropospheric temperatures and global mean temperature in
67 the stratosphere that can be considered when CO₂ concentrations and SSTs are
68 increased together.

69

70 BHP2006 showed that two dynamical relationships held for a set of four idealized
71 climate change simulations in a simplified CCM. First, the negative correlation
72 between zonal mean zonal wind (a proxy for polar vortex strength) and total O₃
73 at Northern Hemisphere (NH) high latitudes in January, as was originally
74 discussed by Braesicke and Pyle (2004). Second, high-latitude temperature was
75 seen to mimic changes in mid-latitude heat flux (the 'tropospheric forcing' by
76 planetary waves) in the December–January–February (DJF) season (e.g., as
77 shown by Newman et al., 2001). This paper will address how warmer SSTs affect
78 the character of these two relationships.

79

80 In the time-slice experiments with present-day SSTs evaluated by BHP2006, it was
81 noted that the behavior of the NH polar vortex (and thus of polar ozone)
82 depended on the background CO₂ concentration: The single-CO₂ experiments
83 responded to ozone depletion in the opposite sense to the doubled CO₂
84 experiments; this effect provided an example of the competition between
85 radiative and dynamical processes in the polar stratosphere. This paper will
86 determine whether increased SSTs enhance cooling in the middle atmosphere,
87 thus favoring stronger polar vortices in all experiments. Do 'future' SSTs affect
88 the coupling between ozone depletion and tropospheric forcing? Sections 3, 4
89 and 5 will assess the response of the UM chemistry-climate model to changes in
90 O₃, CO₂ and SSTs with a set of transport, dynamical, radiative and chemical
91 diagnostics. Section 6 will summarize the main conclusions.

92

93 **2 Methods**

94 **2.1 Model Description**

95 The following discussion refers to a set of eight time–slice integrations conducted
96 with version 4.5.1 of the MetOffice Unified Model (UM). In this configuration, the
97 UM has 3.75° x 2.5° horizontal resolution and 64 vertical levels, with ~1.3km
98 resolution in the stratosphere. The climate model is coupled non-interactively
99 with the Cariolle and Déqué (1986) parameterized stratospheric ozone
100 chemistry scheme. The chemical module contains a cold tracer (X) used to
101 mimic the impact of polar stratospheric clouds (PSCs) on polar ozone: when
102 temperatures drop below a given threshold (~195K for nitric acid trihydrate at
103 50hPa) the cold tracer is produced exponentially with a time constant of four
104 hours; the cold tracer decays with a ten–day time constant. This model setup
105 has been used previously and documented by Braesicke and Pyle (2003, 2004)
106 and Pyle et al. (2005).

107

108 **2.2 Experimental Design**

109 Eight 20–year time–slice experiments will be discussed in this paper (see Table 1).
110 Each experiment tests the combination of one of two CO₂ concentrations
111 (1xCO₂ or 2xCO₂), stratospheric ozone climatologies (1980–like or 2000–like), and
112 SST and sea ice climatologies (present–day or future). Differences between
113 pairs of experiments can be examined so as to isolate the effects of changes in
114 each of the three parameters (ozone, CO₂ and SSTs) on the climate of the
115 middle atmosphere. Since one of the time–slice experiments represents an
116 idealized present–day climate (1B; low CO₂, depleted ozone layer and present–
117 day SSTs) and another represents the likely stratospheric climate in the mid– to
118 late 21st century (2C; high CO₂, recovered ozone layer and future SSTs), the 2C–
119 1B difference can be interpreted as the ‘climate change signal’ (see WMO,
120 2007).

121

122 A 1980–like ozone climatology is prescribed in experiment 1A, whereas a 2000–
123 like ozone climatology, with substantial polar ozone deficits as compared with

124 the 1980-like climatology, is prescribed in experiment 1B. Experiments 1A and 1B
125 use a background CO₂ concentration of 352ppmv. Experiments 2A and 2B are
126 designed to investigate the same change under doubled CO₂ (704ppmv)
127 conditions. As discussed by BHP2006, annually repeating boundary conditions
128 are imposed in all four experiments: AMIP II¹ sea surface temperature (SST) and
129 sea ice climatologies representative of the late 20th century². Volcanic aerosols
130 and the solar cycle are not considered. Experiments 1C to 2D are identical to
131 experiments 1A to 2B, except that they use the 'future' SST climatology
132 described in the next section. The difference in the setup between experiments
133 1A and 1C, for example, is solely a switch from the present-day to the future SST
134 climatology, as is the difference between experiments 1B and 1D, 2A and 2C,
135 and 2B and 2D.

136

137 **2.3 Construction of a 'Future' SST Climatology**

138 Including SSTs as a factor in this study, and thus examining the impact of the
139 ocean surface on the stratospheric chemistry-climate system, requires a 'future'
140 SST climatology. While some CCMs now include an interactive ocean model,
141 UM 4.5.1 is an atmosphere-only model and future SSTs derived from another
142 ocean-atmosphere model simulation must be prescribed. In the present model
143 study, a future SST dataset is constructed by adding a twelve-month set of SST
144 anomalies to the existing present-day SST climatology. A MetOffice SST dataset,
145 spanning from 1970 to 2020, merges HadISST³ data (1970–1995) with SST and sea
146 ice output from HadGEM1 simulations (beginning in 1995). The 'climate change'
147 SST anomalies are defined as the difference between mean SSTs in the 1970s
148 (1971–1980) and mean SSTs the 2010s (2011–2020) from this MetOffice dataset.

148

¹ http://www-pcmdi.llnl.gov/projects/amip/AMIP2EXPDSN/BCS_OBS/amip2_bcs.htm.

² The 'present-day' SST and sea ice climatologies were defined as the AMIP II 1979-1996 mean.

³ <http://hadobs.metoffice.com/hadisst>.

149 The 2010s – 1970s differences are large enough to simulate differences between
150 present-day SSTs and those projected for the mid-21st century, and thus provide
151 a stratospheric response.

152

153 The idealized 'climate change' SST anomalies (i.e. future – present-day) are
154 generally positive. In the tropics and at mid-latitudes, anomalies are of the
155 order of 1–2K (consistent with coupled ocean–atmosphere predictions of SST
156 changes by the mid-21st century; see IPCC, 2007). The largest positive
157 differences occur at high latitudes. Near the Gulfstream and Kuroshio currents,
158 the SST changes exceed 10K; this is larger than predicted by most ocean–
159 atmosphere models (IPCC, 2007). In the tropical Pacific Ocean, the climate
160 change anomalies are positive but small (up to 1.5K) in the Intertropical
161 Convergence Zone (ITCZ), and negligible or slightly negative to the north and
162 south of this region. The strongest positive–negative–positive pattern occurs in
163 the DJF season; this is the pattern of SST anomalies that defines El Niño events.
164 There is a positive trend in the 1970–2020 timeseries of HadGEM1 SSTs in the Niño
165 3.4⁴ region. This finding is in agreement with Timmermann et al. (1999), who
166 predict a climate change–induced shift toward an increasingly positive Niño 3.4
167 index, and thus toward more frequent El Niño events, in future.

168

169 **3 Radiative and Dynamical Response to Changes in Ozone, CO₂** 170 **and SSTs**

171 **3.1 Global Mean Temperature**

172 Profiles of global and annual mean temperature differences allow for an easy
173 assessment of overall radiative changes, suppressing dynamical changes
174 (important at seasonal timescales) and their effects on the thermal structure of
175 the atmosphere. Consistent with Shine et al. (2003, 2008), in the idealized time–

175

⁴ Monthly mean SST anomalies from the 1950–1999 period in the 120°W–170°W, 5°S–5°N region (see Trenberth, 1997).

176 slice experiments, the middle atmosphere cools in response to both ozone
177 depletion (with a small peak in the lower stratosphere and a larger peak
178 centered at 1hPa) and increased CO₂ concentrations (with the strongest
179 cooling at the stratopause). Profiles of the four sets of responses to ozone
180 depletion (Fig. 1, left-hand panel) are indistinguishable from 1000 to 0.1hPa; the
181 responses are the same for both SST climatologies (i.e. 1B-1A ≈ 1D-1C) and for
182 both CO₂ concentrations (1B-1A ≈ 2B-2A). That is, the global mean
183 temperature response to ozone depletion is independent of both background
184 CO₂ and thermal forcing from the sea surface. Similarly, the response to
185 doubled CO₂ (Fig. 1, centre panel) is the same for both ozone climatologies (i.e.
186 2A-1A ≈ 2B-1B) and for either present-day or future SSTs (2A-1A ≈ 2C-1C).

187

188 The troposphere and lower stratosphere are warmer in the future SST
189 experiments than in the experiments using present-day SSTs (Fig. 1, right-hand
190 panel). The magnitude of the SST-related change in global mean stratospheric
191 temperature is far smaller than found for CO₂ doubling or for ozone depletion:
192 Under future SSTs, the troposphere warms as much as 1.3K, while the lower
193 stratosphere warms by ~0.25K. Similarly to the response to ozone depletion and
194 doubled CO₂, the response to the change in SSTs is similar under the differing
195 ozone and CO₂ conditions. Small differences between the four pairs of
196 experiments arise in the upper troposphere/lower stratosphere region, likely due
197 to mismatches in the thermal forcing between the prescribed SSTs and
198 atmospheric greenhouse gas concentrations.

199

200 As in the annual mean, future SSTs enhance warming in the upper
201 troposphere/lower stratosphere region and raise the level where no
202 temperature difference occurs throughout the seasonal cycle (not shown; see
203 Hurwitz, 2008). This finding agrees with previous studies (i.e. Chakrabarty et al.,

204 2001; Fomichev et al., 2007; Lorenz and DeWeaver, 2007) that have found a link
205 between climate change and tropopause height.

206

207 **3.2 Wintertime Lower Stratospheric Temperature, Eddy Heat Flux and** 208 **Geopotential Height**

209 Tropospheric forcing by planetary waves has a large influence on stratospheric
210 temperatures, particularly in winter. Previous studies (e.g., Newman et al., 2001;
211 Austin et al., 2003; Cagnazzo et al., 2006) have used the zonal mean eddy heat
212 flux at 100hPa, averaged over a mid-latitude band (40°N/S and 80°N/S) and
213 over a two-month time period, to diagnose the tropospheric forcing. Fig. 2
214 shows the modeled heat flux with respect to the 50hPa polar temperature. For
215 the NH, December–January (positive) heat flux is plotted against January–
216 February temperature, while for the SH, August–September (negative) heat flux
217 is plotted against September–October temperature. Fig. 2 shows that, for the
218 set of eight experiments, the relationship between tropospheric forcing and
219 polar temperature is linear and positive⁵: Increased tropospheric forcing in the
220 early winter leads to increased polar temperatures at higher altitudes somewhat
221 later in the winter. As expected, Southern polar temperatures are lower (by
222 roughly 20K) than are northern polar temperatures.

223

224 The slopes of the regression lines are steeper in the NH than in the Southern
225 Hemisphere (SH). The mean slope of the eight experiments is 1.29 m⁻¹ s in the NH
226 and -0.80 m⁻¹ s in the SH. These values are in agreement with the analysis by
227 Austin et al. (2003) that found the heat flux–temperature slopes based on the
228 National Centers for Environmental Prediction/National Center for Atmospheric
229 Research (NCEP/NCAR) reanalysis (Kalnay et al., 1996) to be 1.49 ± 0.27 m⁻¹ s
230 (NH) and -0.89 ± 0.16 m⁻¹ s (SH). This result suggests that the NH polar region is

230

⁵ Heat flux is poleward in both hemispheres: positive (negative) values indicate northward (southward) heat flux.

231 more sensitive to changes in tropospheric forcing than is the southern polar
232 region.

233

234 For the NH winter season stronger heat fluxes and lower temperatures are found
235 in experiment 2C (idealized future climate; burgundy) relative to experiment 1B
236 (idealized present-day climate; turquoise). This result agrees with the work of
237 Manzini et al. (2003), who found a downward shift of the heat flux versus
238 temperature regression (perpendicular to the original slopes)) between 1960-like
239 and 2000-like time-slice simulations. In the UM experiments, however, the shift
240 toward stronger heat fluxes and lower temperatures is not significantly larger
241 than the signal due to interannual variability.

242

243 In contrast to the NH, the SH interannual variability is lower, and there is little
244 change in the heat flux and temperature values between the eight
245 experiments. This suggests that the dynamics of the SH stratosphere are not as
246 sensitive to changes in greenhouse gases, SSTs or ozone climatologies, though
247 SH winters are slightly cooler in the doubled-CO₂ experiments. Rather, the SH
248 polar stratosphere is closer to being in radiative equilibrium as compared with
249 the NH.

250

251 As noted by BHP2006, when present-day SSTs are prescribed, DJF heat flux
252 differences due to ozone depletion are positive in a single CO₂ atmosphere (1B-
253 1A) but negative in a doubled CO₂ atmosphere (2B-2A). These differences⁶ are
254 shown in the two leftmost bars in Fig. 3. While the responses to ozone depletion
255 have the opposite sign when future SSTs are prescribed, the 1C-1D heat flux
256 difference is not statistically distinct from the 2D-2C difference. Consistent with
257 the heat flux differences described above, temperature and geopotential

257

⁶ In figure 3, heat flux differences due to ozone depletion are shown as 1A-1B, 2A-2B, etc. as this clarifies the three contributions to the climate change signal, i.e. $2C-1B = (2C-2A) + (2A-1A) + (1A-1B)$.

258 height differences due to ozone depletion are small in the experiments using
259 future SSTs (see Hurwitz, 2008).

260

261 The error bars in Fig. 3 reveal the high degree of interannual variability in
262 tropospheric forcing during the NH winter season, and thus the difficulty in
263 evaluating heat flux differences and their subsequent effects on stratospheric
264 dynamics. The only heat flux differences from that are statistically different from
265 zero are the three changes of parameter relative to experiment 1A (ozone
266 depletion, doubling of CO₂ and increasing SSTs). While heat flux increases due
267 to climate change (2C–1B), dynamical warming of the lower stratosphere is
268 overwhelmed by the radiative cooling associated with doubled CO₂ and
269 increasing SSTs. In the NH winter, 2C–1B temperature and geopotential height
270 differences at 50hPa are generally negative (up to 3K and 30m, respectively;
271 not shown).

272

273 **4 Chemical Response to Changes in Ozone, CO₂ and SSTs**

274 **4.1 Relationship Between Polar Vortex Strength and Ozone at NH High** 275 **Latitudes**

276 The strong relationship between NH polar vortex strength and high–latitude total
277 ozone seen in other CCM experiments (e.g., Braesicke and Pyle, 2004; BHP2006)
278 extends to the four experiments using future SSTs. The slope of the regression line
279 fitting each set of 20 points in experiments 1C through 2D is very similar to that
280 seen in experiments 1A, as is the range of zonal wind and total ozone values
281 (Fig. 4a).

282

283 Fig. 4b shows the mean regression line of all eight 20–year time–slice experiments
284 as well as the mean zonal wind and total ozone values for each experiment. As
285 noted by BHP2006, experiments where present–day SSTs are prescribed (1A–2B)
286 exhibit a ‘flip flop’ response to ozone depletion. The means of the future SST

287 experiments (1C through 2D) are situated between these two states (1A/2B and
288 1B/2A); differences in the mean zonal winds and ozone in the future SST
289 experiments are not statistically significant.

290

291 **4.2 Polar Ozone Loss as a Function of PSC Volume**

292 Rex et al. (2004, 2006) found a linear relationship between column ozone loss
293 and PSC volume during the NH winter, in observations of the past two decades.
294 BHP2006 examined this same relationship in four UM experiments using present-
295 day SSTs (1A–2B). The strongest correlation between ozone loss and PSC volume
296 was found in experiment 1A (1980-like ozone and 1xCO₂; $r = 0.98$), while
297 somewhat weaker linear relationships were found in two other experiments (1B
298 and 2A). In experiment 2B (2000-like ozone and 2xCO₂), ozone losses were
299 clustered around 90DU despite interannual variation in PSC volumes and polar
300 temperatures.

301

302 The relationship between ozone loss and PSC volume is examined in the future
303 SST experiments (1C–2D). Just as for experiments 1A–2B, PSC volume is defined
304 as the sum of all grid cells where cold tracer values exceed a fixed threshold
305 (0.95). For each time-slice experiment and for each winter season, the DJF
306 average PSC volume is then sorted into size classes (bin width $\Delta = 1 \cdot 10^7 \text{ km}^3$; bin
307 overlap $\delta = 0.5 \cdot 10^7 \text{ km}^3$). Also, the modeled January mean polar temperature
308 (at 30hPa, north of 85°N), and the wintertime column ozone loss from November
309 to March (within the 400 to 550K potential temperature layer) are calculated for
310 each winter and sorted according to the associated PSC volume size class. The
311 linear relationship between ozone loss and DJF PSC volume in experiments 1C
312 and 2D (1A and 2B with future SSTs) have slopes nearly identical to that found in
313 1A and a good fit ($r \sim 0.85$). Another of the future SSTs experiments (1D) has a
314 similar slope but a lower correlation coefficient. The idealized future climate

315 scenario (2C) exhibits the same 'saturation' behavior as does experiment 2B:
316 wintertime column ozone losses do not correlate with PSC volumes.

317

318 In the NH winter, PSC volumes and polar temperatures are related by a power
319 law. The highest mean wintertime PSC volumes generally correspond with the
320 lowest mean January polar temperatures, as PSC formation is highly
321 temperature-dependent. Three of the future SST experiments have continuous
322 temperature distributions, similarly to experiment 1A (refer to BHP2006, Fig. 7).
323 The idealized future climate scenario (2C) has a bimodal distribution, as seen in
324 two of the experiments with present-day SSTs (1B and 2A).

325

326 **5 Sensitivity of the Brewer–Dobson Circulation to Ozone Depletion** 327 **and Climate Change**

328 Tropospheric forcing changes in response to ozone depletion/recovery and
329 climate change, particularly during the NH winter season, are likely to be linked
330 to changes in the strength of the Brewer–Dobson circulation (BDC; originally
331 described by Brewer (1949) and Dobson (1956)). Tropospheric forcing correlates
332 not only with stratospheric mid-winter temperatures in the lower stratosphere
333 (e.g., as shown in Fig. 2) and with polar ozone, but is also connected to the
334 residual circulation in the middle atmosphere. Newman et al. (2001) calculated
335 that a 10% reduction in the 100hPa eddy heat flux would weaken the BDC by
336 10%. Conversely, recent increases in tropospheric forcing (as discussed by
337 Dhomse et al., 2006) may have caused a strengthening of the stratospheric
338 circulation. Modeling studies by Butchart and Scaife (2001), Austin and Li (2006)
339 and Li et al. (2008) have shown that increased greenhouse gas concentrations
340 lead to a strengthened BDC in the middle atmosphere. Increased heating near
341 the equator and thus increased upward mass flux in the tropics is a key part of
342 the mechanism that links greenhouse gas concentrations with a stronger
343 Brewer–Dobson circulation (Eichelberger and Hartmann, 2005). Butchart and

344 Scaife (2001) and Li et al. (2008) found increased tropical upwelling in
345 conjunction with increased downwelling at high latitudes, in climate change
346 simulations, but could not provide an unambiguous mechanism for the
347 strengthening. Climate change-related strengthening of the BDC has not been
348 observed as yet (Engel et al., 2009).

349

350 The present study will separate the effects of each parameter change (ozone
351 depletion/recovery, increased greenhouse gas concentrations and increased
352 SSTs) on the strength and character of the BDC. This study complements a
353 recent study by Oman et al. (2009), which examined changes in the age of
354 stratospheric air in transient simulations of the recent past and future.

355

356 **5.1 Qualitative Streamfunction Analysis**

357 For each of the eight time-slice experiments, the residual streamfunction is
358 calculated following Andrews et al. (1987). A latitude-height cross-section of
359 the residual streamfunction in the idealized present-day climate simulation (1B),
360 for the DJF season, is shown in Fig. 5a. Many features of the observed meridional
361 circulation are reproduced: first, the separation of transport toward the South
362 Pole (negative contours) from transport toward the North Pole (positive
363 contours) is located just south of the equator (due to the southward shift of the
364 ITCZ during the NH winter season). The strongest transport occurs in the
365 troposphere; the Hadley and Ferrell cells can be seen in the tropics and at mid-
366 latitudes, respectively, and in both hemispheres. The larger but weaker BDC (i.e.
367 following the $\pm 0.1 \text{ kg s}^{-3}$ contours) is characterized by upwelling in the tropics,
368 poleward transport through the stratosphere, and downwelling at high latitudes
369 (particularly in the NH, during the DJF season). Mesospheric transport also
370 features equatorial upwelling and downwelling at high latitudes of the winter
371 hemisphere, though the winter pole is favored.

372

373 Pressure-weighting the streamfunction highlights the behavior of the middle
374 atmosphere; an example is shown in Fig. 5b. In experiment 1B, during the DJF
375 season, the largest magnitudes occur above 5hPa, with another region of strong
376 upwelling in the equatorial upper troposphere.

377

378 For an in depth comparison of streamfunction values, seven regions are defined.
379 As shown in Fig. 5b, these regions provide good coverage of the features of the
380 BDC. Each of the seven boxes covers a 20° latitude band and spans four model
381 pressure levels. Region 1 is located in the equatorial lower stratosphere (10°S to
382 10°N). Regions 2, 3 and 4 are located in the upper stratosphere; region 3 is
383 centered at the equator, while regions 2 and 4 are located in the SH and NH
384 high latitudes (60° to 80° latitude) respectively. Regions 5, 6 and 7 are located in
385 the mesosphere, region 6 at the equator, and regions 5 and 7 in the SH and NH
386 mid- to high latitudes (40° to 60° latitude).

387

388 Seasonal differences in pressure-weighted streamfunction values generally have
389 the same sign in the equatorial upper troposphere (region 1) as in the
390 mesosphere (regions 5, 6 and 7; not shown). Doubling the background CO₂
391 concentration (for example, 2A–1A or 2C–1B) leads to small changes in
392 streamfunction values in the equatorial UT/LS and larger changes in the upper
393 stratosphere, in the winter hemisphere. These streamfunction changes are
394 positive in the DJF and MAM seasons, but negative in the JJA and SON seasons;
395 streamfunction changes in the NH winter are generally larger than in the SH
396 winter. The difference between the two ozone climatologies (i.e. the difference
397 between experiments 1A and 1B) has little effect on streamfunction values in the
398 troposphere and stratosphere; changes in the mesosphere tend to be smaller
399 than for the difference seen when the background CO₂ concentration is
400 doubled. For the change from the present-day to the future SST climatology,
401 streamfunction values increase (decrease) during the NH (SH) winter. The

402 magnitude of the changes is larger in the upper troposphere than in the middle
403 atmosphere.

404

405 While this initial, qualitative analysis hints at the influence of CO₂, O₃ and forcing
406 from the ocean surface on tropical upwelling and the overturning circulation in
407 the middle atmosphere, a more quantitative approach (which follows)
408 evaluates the relative importance of changes in these three parameters, as well
409 as their variation with altitude and season, on the strength of the BDC under
410 climate change.

411

412 **5.2 Quantifying Seasonal Differences in the Mean Streamfunction**

413 The impact of changes in ozone, CO₂ and SSTs on the seasonal mean strength
414 of the meridional overturning circulation is assessed quantitatively by grouping
415 together pairs of experiments differing by the same boundary conditions. In Fig.
416 6, the bars shown in blue represent pairs of experiments which differ only by their
417 O₃ climatology (1980-like – 2000-like); the pink bars represent pairs of
418 experiments which differ only by their background CO₂ concentration (704ppmv
419 – 352ppmv); the green bars represent pairs of experiments which differ only by
420 their SST climatology (future – present-day); the yellow bars represent the
421 climate change signal (2C–1B). Positive values (increased streamfunction)
422 indicate increased transport toward the North Pole, whereas negative values
423 (decreased streamfunction) indicate increased transport toward the South Pole.
424 Values not significantly different from zero indicate that changing a particular
425 parameter has not affected the meridional circulation. Error bars shown in
426 region 5 (in Fig. 6) denote ± 1 standard deviation; often, the uncertainties are
427 comparable to the magnitudes of the differences themselves.

428

429 Fig. 6 shows pressure-weighted streamfunction differences between pairs of
430 experiments, in the seven atmospheric regions defined in section 5.1, for the DJF

431 season. Streamfunction values are larger in the idealized future climate
432 scenario (experiment 2C) than in the idealized present-day climate (1B).
433 Furthermore, this figure shows that the relative contribution of the three types of
434 parameter changes is altitude dependent. The SST change dominates the
435 climate change signal in the upper troposphere (region 1) while the CO₂
436 change dominates in the NH high-latitude upper stratosphere (region 4), and
437 the CO₂ and O₃ changes dominate in the mesosphere (regions 5–7).

438

439 Streamfunction differences have a seasonal cycle. Streamfunction differences
440 are generally positive in the DJF season (i.e., increased transport toward the
441 North Pole; see Fig. 6) and negative in the June–July–August (JJA) season
442 (increased transport toward the South Pole; not shown). That is, the strength of
443 the meridional circulation increases in both the NH and SH winter seasons.
444 Generally, differences are positive in the March–April–May (MAM) season and
445 negative in the September–October–November (SON) season, though the
446 magnitudes of these differences are smaller than in the two winter seasons. In
447 regions 2 and 4 (located in the high-latitude upper stratosphere), pressure-
448 weighted streamfunction magnitudes in each of the simulations are small (see
449 Fig. 5b) and the seasonal cycles are much weaker than in other parts of the
450 atmosphere.

451

452 **5.3 Relationship Between Tropical Upwelling and Polar Ozone**

453 Time-slice simulations with increased CO₂ predict that the polar vortex will
454 strengthen and, assuming the continued presence of anthropogenic chlorine,
455 greater wintertime ozone loss should occur by the mid- to late 21st century (note
456 the differences between 2C and 1B in Fig. 4). The same simulations predict that
457 the strength of the BDC will increase as greenhouse gas concentrations
458 continue to rise and the ozone layer recovers (see Fig. 6). Combining these two

459 predictions, increased tropical upwelling in early or mid-winter should correlate
460 with a decrease in total column ozone at NH high latitudes in late winter.

461

462 For individual time-slice experiments, the correlation between tropical
463 streamfunction and high-latitude total ozone is low, due to the high degree of
464 interannual variability within the 20-year analysis period; García-Herrera et al.
465 (2006) note that relating changes in tropical upwelling and circulation changes
466 at high latitudes is made difficult because of various sources of climate
467 variability, such as the quasi-biennial oscillation (QBO). A more robust
468 relationship between tropical upwelling and polar ozone emerges when the
469 means of each experiment are examined (Fig. 7). As expected, least squares
470 fitting of the eight means yields a negative slope; that is, relative to present-day
471 (experiment 1B), there will be stronger tropical upwelling but lower total ozone
472 near the north pole in March in a future climate (2C)⁷. Though differences
473 between experiments 1B and 2C are statistically significant, the linear regression
474 of January pressure-weighted streamfunction in region 3 as a function of March
475 total ozone at 80°N (Fig. 7) is not.

476

477 Correlations of the annual cycles of the pressure-weighted streamfunction
478 between two of the seven atmospheric regions are much higher (generally
479 exceeding 0.90; see Hurwitz, 2008) than for the tropical streamfunction-polar
480 ozone link. That is, increased tropical upwelling corresponds with increased
481 meridional transport in the mesosphere. (Correlations with region 2, which is
482 outside the region of meridional overturning circulation for much of the year, are
483 not statistically significant.) The magnitude of these correlations is generally
484 consistent from experiment to experiment. Thus, although the strength of the
485 BDC is likely to be affected by changes in greenhouse gas concentrations and

485

⁷ Note that this result is a dynamical signature and does not take into account potential changes in ozone chemistry.

486 other climate forcings, the structure of the circulation pattern itself will remain
487 unchanged.

488

489 **6 Discussion**

490 This study assessed the roles of three contributors to future stratospheric climate
491 change: increasing CO₂, ozone recovery and generally warmer sea surface
492 temperatures. Stratospheric temperatures, dynamics, ozone and the strength of
493 the Brewer-Dobson circulation were examined in various idealized climate
494 scenarios, using a chemistry–climate model with parameterized ozone
495 chemistry. The ‘climate change’ signal (2C–1B), the difference from an
496 idealized present–day climate and one predicted for the mid– to late 21st
497 century, corresponded with an increase in polar vortex strength, increased
498 poleward heat fluxes, decreases in stratospheric temperature and a
499 strengthening of the BDC.

500

501 In experiments where future SSTs were prescribed (1C–2D; see Table 1), the
502 global mean temperature responses to decreased ozone and increased CO₂
503 concentrations matched those seen in experiments using present–day SSTs (see
504 Fig. 1). In the stratosphere, the SST–related global mean temperature response
505 was weaker than was the response to doubling CO₂ or to ozone depletion.
506 Nevertheless, the switch from present–day to future SSTs enhanced tropospheric
507 warming and slightly increased global mean temperatures in the lower
508 stratosphere, elevating the tropopause.

509

510 A time–lagged linear relation between heat flux and temperature held for all
511 eight time–slice experiments in both winter seasons (see Fig. 2). The NH and SH
512 heat flux–temperature relationships had different slopes, though both showed a
513 positive association between poleward heat fluxes in the upper troposphere

514 and increased polar temperatures in the lower stratosphere. SH dynamics were
515 less sensitive to changes in CO₂, O₃ and SSTs than were NH dynamics.

516

517 As noted by BHP2006, the response to ozone depletion was CO₂-dependent:
518 the NH stratospheric vortex weakened under present-day CO₂ conditions (1B-
519 1A) but strengthened in a doubled-CO₂ atmosphere (2B-2A). This 'flip flop'
520 response was not seen in the four experiments where future SSTs were
521 prescribed. Under future SSTs, prescribed ozone depletion had no significant
522 effect on temperatures, heat fluxes, ozone concentrations or zonal winds at NH
523 high latitudes in winter. This may have resulted from the reduction in
524 baroclinicity in the atmosphere, when SSTs and greenhouse gas concentrations
525 were increased simultaneously.

526

527 A strong anti-correlation between 10hPa zonal wind at 60°N and total ozone at
528 80°N is common to experiments using present-day SSTs (BHP2006) and to the
529 future SST experiments. The lines of best fit were nearly identical. That the
530 relationship between polar vortex strength and polar ozone remained robust,
531 despite large changes in the temperature structure and dynamics of the middle
532 atmosphere, points to the fundamental interdependence of chemistry and
533 climate in the NH polar stratosphere.

534

535 Changes in tropical upwelling and meridional overturning in the middle
536 atmosphere were quantified by examining regional streamfunction variations.
537 In the model experiments, increased tropical upwelling, reduced mid-winter
538 polar ozone and increased polar vortex strength occurred in a climate forced
539 by warmer SSTs and higher greenhouse gas concentrations. The idealized
540 climate change signal (2C-1B) showed a strengthened streamfunction,
541 particularly for the DJF and JJA seasons. This result, therefore, is consistent with
542 previous modeling studies that suggest that the BDC will strengthen in a future

543 climate. The relative contribution of SSTs, O₃ and CO₂ changes to the enhanced
544 circulation in the middle atmosphere was altitude dependent: SST changes
545 played an important role in the tropical upper troposphere (consistent with
546 Garny et al. (2009)), while changes in CO₂ and O₃ dominated the circulation
547 response in the middle atmosphere (see Fig. 6).

548

549 This work predicted no substantial change in the relationship between
550 tropospheric forcing, polar temperature and BDC in a future climate. However,
551 it was not possible to relate climate change-induced increases in tropical
552 upwelling in mid-winter to greater springtime ozone losses at NH high latitudes at
553 statistically significant levels.

554

555 **Acknowledgements**

556 M. M. Hurwitz would like to acknowledge funding from Emmanuel College,
557 Cambridge and from the NASA Postdoctoral Program at Goddard Space Flight
558 Center, administered by Oak Ridge Associated Universities through a contract
559 with NASA. P. Braesicke and J. A. Pyle acknowledge NERC funding through
560 NCAS. The authors thank NCAS-CMS for computational support.

561

561 **References**

562

563 Andrews, D. G., J. R. Holton, and C. B. Leovy, 1987: *Middle Atmosphere*
564 *Dynamics*. Academic Press, 489pp.

565

566 Austin, J., and Coauthors, 2003: Uncertainties and assessments of chemistry-
567 climate models of the stratosphere. *Atmos. Chem. Phys.*, **3**, 1–27.

568

569 Austin, J., and F. Li, 2006: On the relationship between the strength of the
570 Brewer–Dobson circulation and the age of stratospheric air. *Geophys. Res. Lett.*,
571 **33**, L17807.

572

573 Braesicke, P., M. M. Hurwitz, and J. A. Pyle, 2006: The Stratospheric response to
574 changes in ozone and carbon dioxide as modelled with a GCM including
575 parameterized stratospheric chemistry. *Meteorol. Z.*, **15**, 343–354.

576

577 Braesicke, P., and J. A. Pyle, 2003: Changing ozone and changing circulation in
578 northern mid-latitudes: Possible feedbacks? *Geophys. Res. Lett.*, **30**, 1059.

579

580 Braesicke, P., and J. A. Pyle, 2004: Sensitivity of dynamics and ozone to different
581 representations of SSTs in the Unified Model. *Q. J. R. Meteorol. Soc.*, **130**, 2033–
582 2045.

583

584 Brewer, A. W., 1949: Evidence for a world circulation provided by the
585 measurements of helium and water vapour distribution in the stratosphere. *Q. J.*
586 *R. Meteorol. Soc.*, **75**, 351–363.

587

588 Butchart, N., and A. A. Scaife, 2001: Removal of chlorofluorocarbons by
589 increased mass exchange between the stratosphere and troposphere in a
590 changing climate. *Nature*, **410**, 799–802.

591

592 Cagnazzo, C., C. Claud, and S. Hare, 2006: Aspects of stratospheric long-term
593 changes induced by ozone depletion. *Climate Dynamics*, **27**, 101–111.

594

595 Cariolle, D., and M. Déqué, 1986: Southern Hemisphere Medium-Scale Waves
596 and Total Ozone Disturbances in a Spectral General Circulation Model. *J.*
597 *Geophys. Res.*, **91**, 10825–10846.

598

599 Chakrabarty, D. K., K. V. Pandya, and N. C. Shah, 2001: Long-term trend of
600 tropopause. *Advances in Space Research*, **28**, 981–986.

601

602 Dhomse, S., M. Weber, I. Wohltmann, M. Rex, and J. P. Burrows, 2006: On the
603 possible causes of recent increases in northern hemispheric total ozone from a
604 statistical analysis of satellite data from 1979 to 2003. *Atmos. Chem. Phys.*, **6**,
605 1165–1180.

606

607 Dobson, G. M. B., 1956: Origin and distribution of the polyatomic molecules in
608 the atmosphere. *Proc. Roy. Soc. A*, **236**, 187–193.

609

610 Eichelberger, S. J., and D. L. Hartmann, 2005: Changes in the strength of the
611 Brewer–Dobson circulation in a simple AGCM. *Geophys. Res. Lett.*, **32**, L15807.

612

613 Engel, A., and Coauthors, 2009: Age of air unchanged within uncertainties over
614 the past 30 years. *Nature Geoscience*, **2**, 28–31.

615

616 Fomichev, V. I., A. I. Jonsson, J. DeGrandpré, S. R. Beagley, C. McLandress, K.
617 Semeniuk, and T. G. Shepherd, 2007: Response of the middle atmosphere to
618 CO₂ doubling: Results from the Canadian Middle Atmosphere Model. *J.*
619 *Climate*, **20**, 1121–1144.

620

621 García-Herrera, R., N. Calvo, R. R. Garcia, and M. A. Giorgetta, 2006:
622 Propagation of ENSO temperature signals into the middle atmosphere: A
623 comparison of two general circulation models and ERA-40 reanalysis data. *J.*
624 *Geophys. Res.*, **111**, D06101.

625

626 Garny, H., M. Dameris, and A. Stenke, 2009: Impact of prescribed SSTs on
627 climatologies and long-term trends in CCM simulations. *Atmos. Chem. Phys.*
628 *Discuss.*, **9**, 4489–4524.

629

630 Hurwitz, M. M., 2008: *Idealised Numerical Simulations of the Stratospheric*
631 *Chemistry–Climate System*. PhD Thesis, University of Cambridge, 203pp.

632

633 Intergovernmental Panel on Climate Change (IPCC), 2007: *Climate Change*
634 *2007: The Scientific Basis: Contribution of Working Group I to the Fourth*
635 *Assessment Report of the Intergovernmental Panel on Climate Change*, edited
636 by J. T. Houghton et al., Cambridge Univ. Press.

637

638 Johns, T. C., and Coauthors, 2003: Anthropogenic climate change for 1860 to
639 2100 simulated with the HadCM3 model under updated emissions scenarios.
640 *Climate Dynamics*, **20**, 583–612.

641

642 Kalnay, E., and Coauthors, 1996: The NCEP/NCAR 40-year reanalysis project. *B.*
643 *Am. Meteorol. Soc.*, **77**, 437–471.

644

645 Li, F., J. Austin, and J. Wilson, 2008: The Strength of the Brewer–Dobson
646 Circulation in a Changing Climate. *J. Climate*, **21**, 40–57.

647

648 Lorenz, D. J., and E. T. DeWeaver, 2007: Tropopause height and zonal wind
649 response to global warming in the IPCC scenario integrations. *J. Geophys. Res.*,
650 **112**, D10119.

651

652 Manzini, E., B. Steil, C. Bruehl, M. A. Giorgetta, and K. Kruger, 2003: A new
653 interactive chemistry–climate model: 2. Sensitivity of the middle atmosphere to
654 ozone depletion and increase in greenhouse gases and implications for recent
655 stratospheric cooling. *J. Geophys. Res.*, **108**, 4429.

656

657 Newman, P. A., E. R. Nash, and J. E. Rosenfield, 2001: What controls the
658 temperature of the Arctic stratosphere during the spring? *J. Geophys. Res.*, **106**,
659 19999–20010.

660

661 Oman, L. D., D. W. Waugh, S. Pawson, R. S. Stolarski, and P. A. Newman, 2009:
662 On the influence of anthropogenic forcings on changes in the stratospheric
663 mean age, *J. Geophys. Res.*, **114**, D03105, doi:10.1029/2008JD010378.

664

665 Pyle, J. A., P. Braesicke and G. Zeng, 2005: Dynamical variability in the modelling
666 of chemistry–climate interactions. *Faraday Discussions*, **130**, 27–39.

667

668 Rex, M., R. J. Salawitch, P. von der Gathen, N. P. R. Harris, M. P. Chipperfield, and
669 B. Naujokat, 2004: Arctic ozone loss and climate change. *Geophys. Res. Lett.*,
670 **31**, L04116.

671

672 Rex, M., and Coauthors, 2006: Arctic winter 2005: Implications for stratospheric
673 ozone loss and climate change, *Geophys. Res. Lett.*, **33**, L23808,
674 doi:10.1029/2006GL026731.

675

676 Shine, K. P., J. J. Barnett, and W. J. Randel, 2008: Temperature trends derived
677 from Stratospheric Sounding Unit radiances: The effect of increasing CO₂ on the
678 weighting function. *Geophys. Res. Lett.*, **35**, L02710.

679

680 Shine, K. P., and Coauthors, 2003: A comparison of model-simulated trends in
681 stratospheric temperatures. *Q. J. R. Meteorol. Soc.*, **129**, 1565–1588.

682

683 Timmermann, A., J. Oberhuber, A. Bacher, M. Esch, M. Latif, and E. Roeckner,
684 1999: Increased El Niño frequency in a climate model forced by future
685 greenhouse warming. *Nature*, **398**, 694–697.

686

687 Trenberth, K. E., 1997: The Definition of El Niño. *B. Am. Meteorol. Soc.*, **78**, 2771–
688 2777.

689

690 World Meteorological Organisation (WMO), 2007: *Scientific assessment of ozone*
691 *depletion: 2006*, Global Ozone Res. And Monitor. Proj. Rep. 50, Geneva,
692 Switzerland.

693

693 **Figure Captions**

694

695 **Table 1:** Experimental design.

696

697 **Figure 1:** Summary of global and annual mean temperature response for the set
698 of eight time-slice experiments. The left-hand panel shows the ozone-related
699 response (2000-like – 1980-like); the turquoise line shows 1B–1A differences, the
700 yellow line shows 2B–2A differences, the pink line shows 1D–1C differences and
701 the light grey line shows 2D–2C differences. The central panel shows the CO₂-
702 related response (2xCO₂ – 1xCO₂); the orange line shows 2A–1A differences, the
703 yellow line shows 2B–1B differences, the dark grey line shows 2C–1C differences
704 and the light grey line shows 2D–1D differences. The right-hand panel shows the
705 SST-related response (future – present-day); the burgundy line shows 1C–1A
706 differences, the pink line shows 1D–1B differences, the dark grey line shows 2C–
707 2A differences and the light grey line shows 2D–2B differences.

708

709 **Figure 2:** Zonal mean meridional mid-latitude heat flux at 100hPa versus polar
710 temperature at 50hPa. For the NH winter, heat fluxes are northward (positive);
711 the scatter plot shows December–January heat fluxes versus January–February
712 temperatures for each year of each experiment. For the SH winter, heat fluxes
713 are southward (negative); the scatter plot shows July–August heat fluxes versus
714 August–September temperatures. Experiment 1A is shown in blue, 1B in
715 turquoise, 2A in orange, 2B in yellow, 1C in burgundy, 1D in pink, 2C in dark grey
716 and 2D in light grey; refer to table 1.

717

718 **Figure 3:** DJF 100hPa heat flux differences between pairs of experiments. The
719 blue bars show heat flux differences due to ozone recovery (1980-like – 2000-
720 like); the pink bars show heat flux differences due to doubling CO₂; the green

721 bars show heat flux differences due to SSTs (future – present–day); the yellow bar
722 shows the climate change signal (2C–1B).

723

724 **Figure 4:** a) Scatter plot of January zonal mean zonal wind versus total ozone for
725 experiments 1A, 1C, 1D, 2C and 2D. b) Scatter plot of the 20–year mean
726 January zonal wind versus total ozone for all eight time–slice experiments. The
727 dotted line shows the mean regression line relating zonal wind to total ozone.

728

729 **Figure 5:** (a) Latitude–height cross–section showing the mean streamfunction for
730 experiment 1B, for the DJF season [1×10^{-9} kg/s³]. (b) Latitude–height cross–
731 section of the mean pressure–weighted streamfunction (the streamfunction
732 divided by the pressure in hPa) for experiment 1B for the DJF season [1×10^{-9} m/s].
733 The seven numbered boxes identify the atmospheric regions defined in section
734 5.1 of the text.

735

736 **Figure 6:** Pressure–weighted streamfunction differences between pairs of
737 experiments, for seven atmospheric regions, for the DJF season. The spatial
738 organization of the regions is as shown in figure 6b. The four bars for each set of
739 differences denote the DJF, MAM, JJA and SON seasons, respectively. The blue
740 bars represent the response to ozone recovery; the pink bars represent the
741 response to doubled CO₂; the green bars represent the response to increased
742 SSTs; the yellow bars represent the response in the climate change signal (2C–
743 1B). Error bars in region 5 denote ± 1 standard deviation.

744

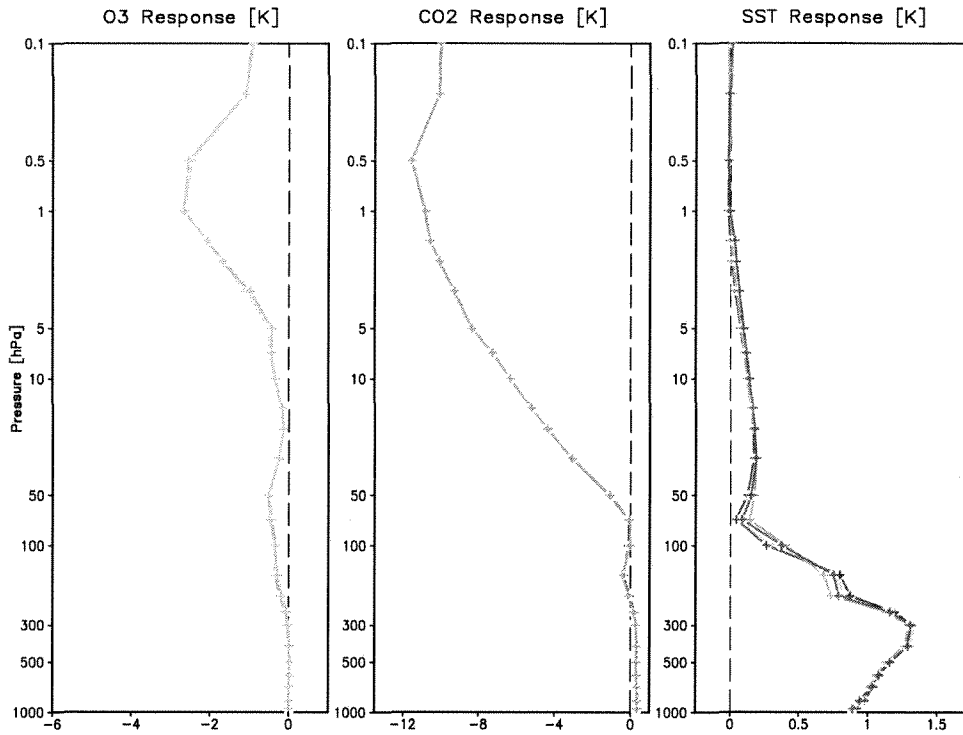
745 **Figure 7:** January streamfunction in region 3 versus March total column ozone at
746 80°N. The colored circles show the 20–year mean for each time–slice
747 experiment; the dashed line shows the line of best fit, fitting the eight mean
748 values.

749 **Figures**

Experiment	O ₃ Climatology	Background [CO ₂] (ppmv)	SST Climatology
1A	1980	352 (1xCO ₂)	Present-day
1B	2000	352	Present-day
2A	1980	704 (2xCO ₂)	Present-day
2B	2000	704	Present-day
1C	1980	352	Future
1D	2000	352	Future
2C	1980	704	Future
2D	2000	704	Future

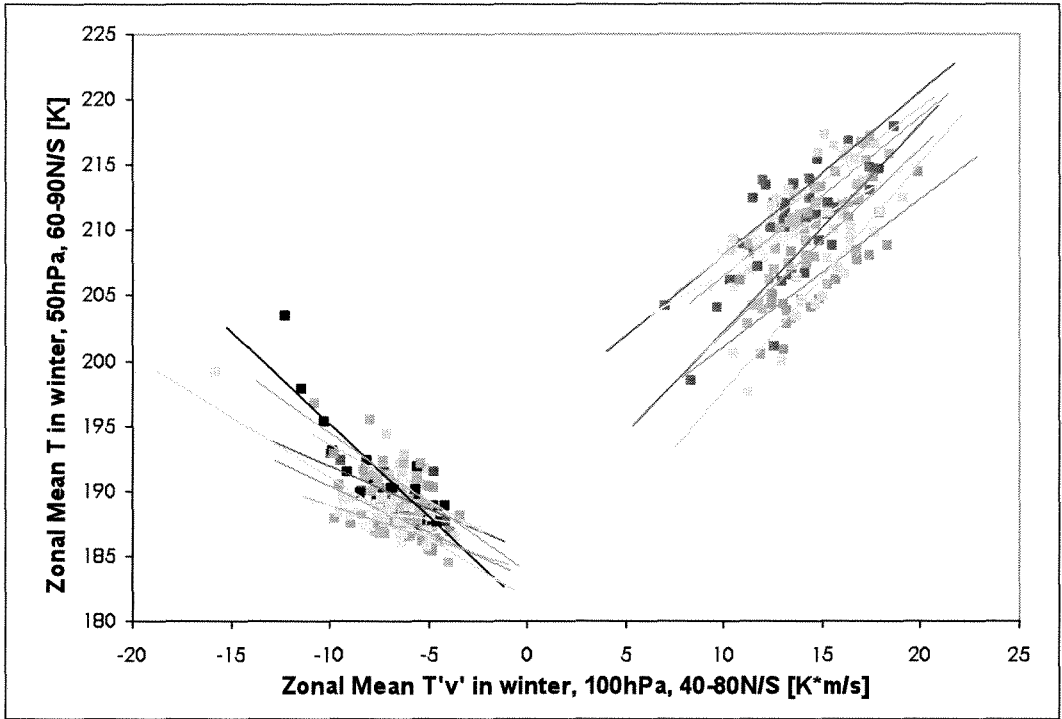
Table 1: Experimental design.

750
 751



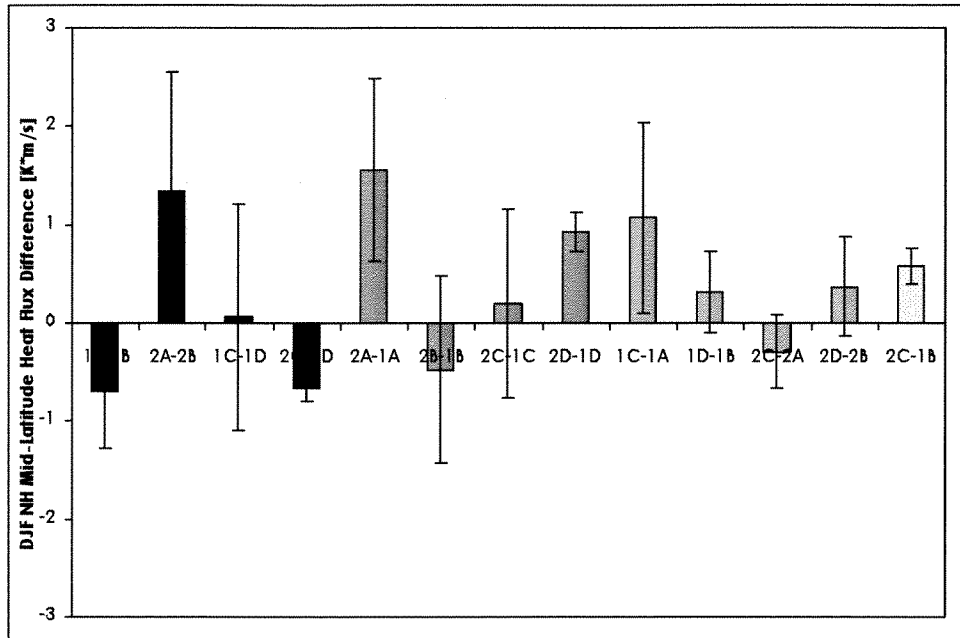
751

752 **Figure 1:** Summary of global and annual mean temperature response for the set
753 of eight time-slice experiments. The left-hand panel shows the ozone-related
754 response (2000-like – 1980-like); the turquoise line shows 1B–1A differences, the
755 yellow line shows 2B–2A differences, the pink line shows 1D–1C differences and
756 the light grey line shows 2D–2C differences. The central panel shows the CO₂-
757 related response (2xCO₂ – 1xCO₂); the orange line shows 2A–1A differences, the
758 yellow line shows 2B–1B differences, the dark grey line shows 2C–1C differences
759 and the light grey line shows 2D–1D differences. The right-hand panel shows the
760 SST-related response (future – present-day); the burgundy line shows 1C–1A
761 differences, the pink line shows 1D–1B differences, the dark grey line shows 2C–
762 2A differences and the light grey line shows 2D–2B differences.



763

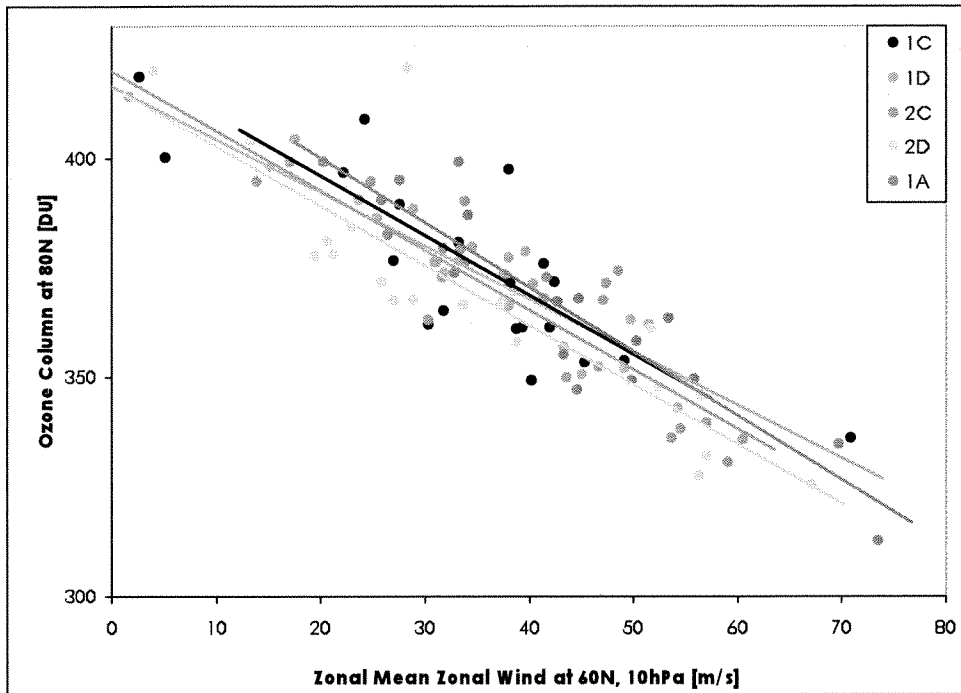
764 **Figure 2:** Zonal mean meridional mid-latitude heat flux at 100hPa versus polar
765 temperature at 50hPa. For the NH winter, heat fluxes are northward (positive);
766 the scatter plot shows December–January heat fluxes versus January–February
767 temperatures for each year of each experiment. For the SH winter, heat fluxes
768 are southward (negative); the scatter plot shows July–August heat fluxes versus
769 August–September temperatures. Experiment 1A is shown in blue, 1B in
770 turquoise, 2A in orange, 2B in yellow, 1C in burgundy, 1D in pink, 2C in dark grey
771 and 2D in light grey; refer to table 1.



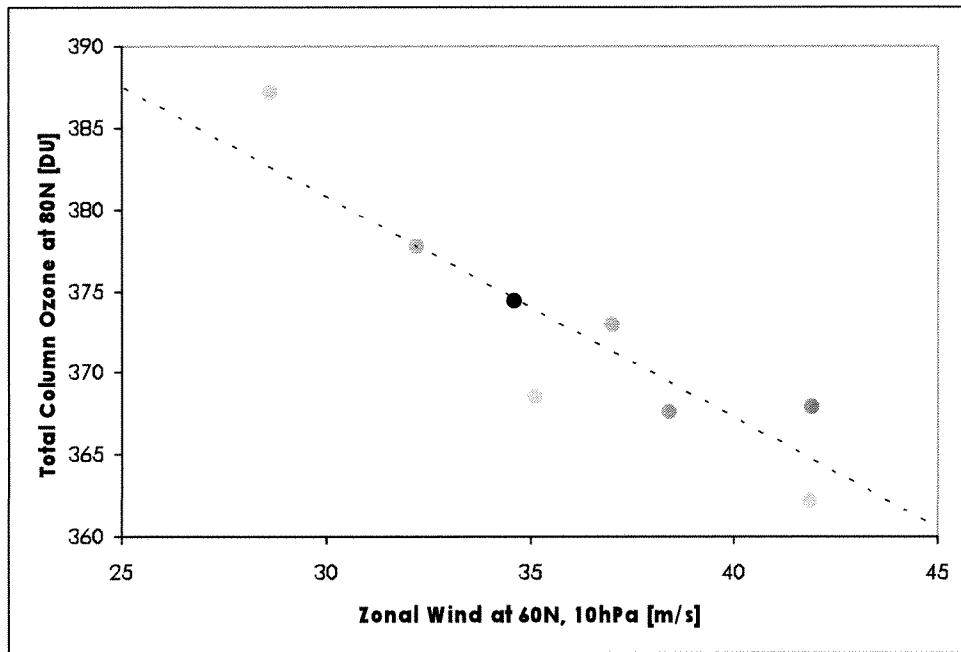
772

773 **Figure 3:** DJF 100hPa heat flux differences between pairs of experiments. The
774 blue bars show heat flux differences due to ozone recovery (1980-like – 2000-
775 like); the pink bars show heat flux differences due to doubling CO₂; the green
776 bars show heat flux differences due to SSTs (future – present-day); the yellow bar
777 shows the climate change signal (2C-1B).

778

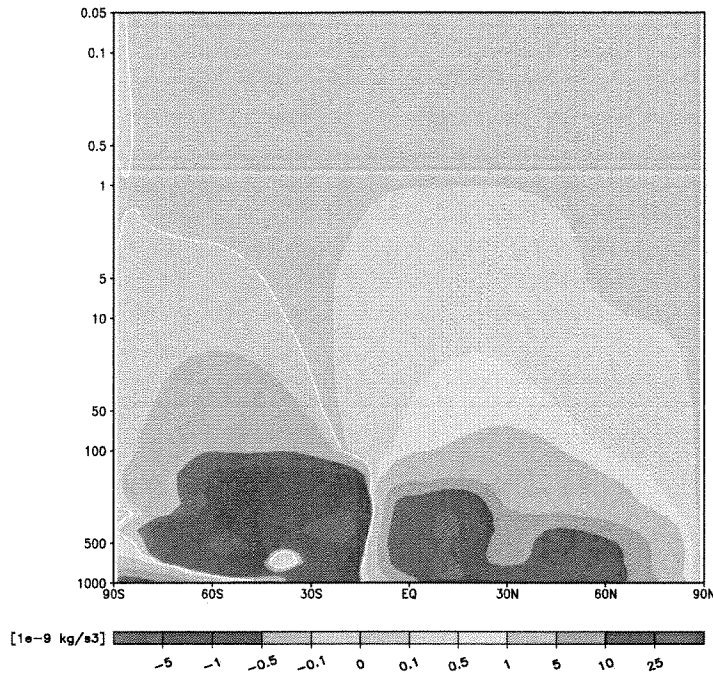


778 a)

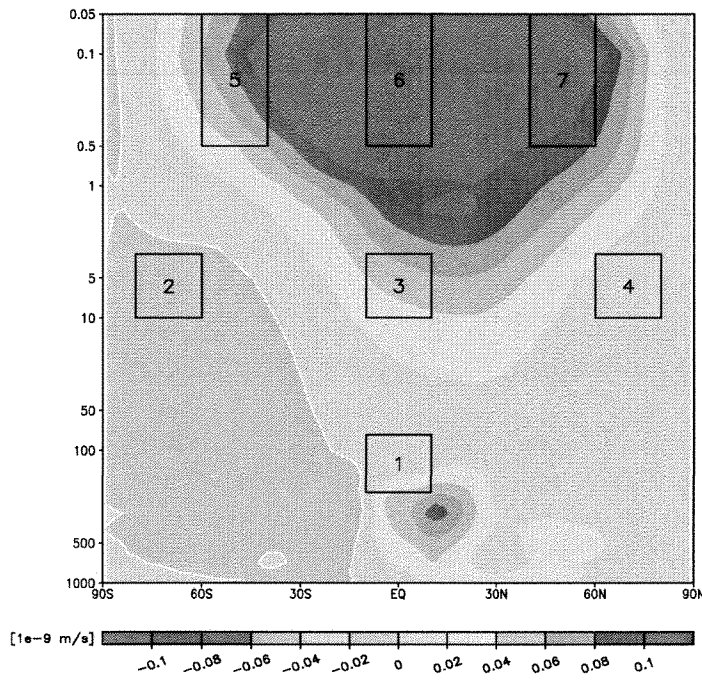


779 b)

780 **Figure 4:** a) Scatter plot of January zonal mean zonal wind versus total ozone for
781 experiments 1A, 1C, 1D, 2C and 2D. b) Scatter plot of the 20-year mean
782 January zonal wind versus total ozone for all eight time-slice experiments. The
783 dotted line shows the mean regression line relating zonal wind to total ozone.



784 a)

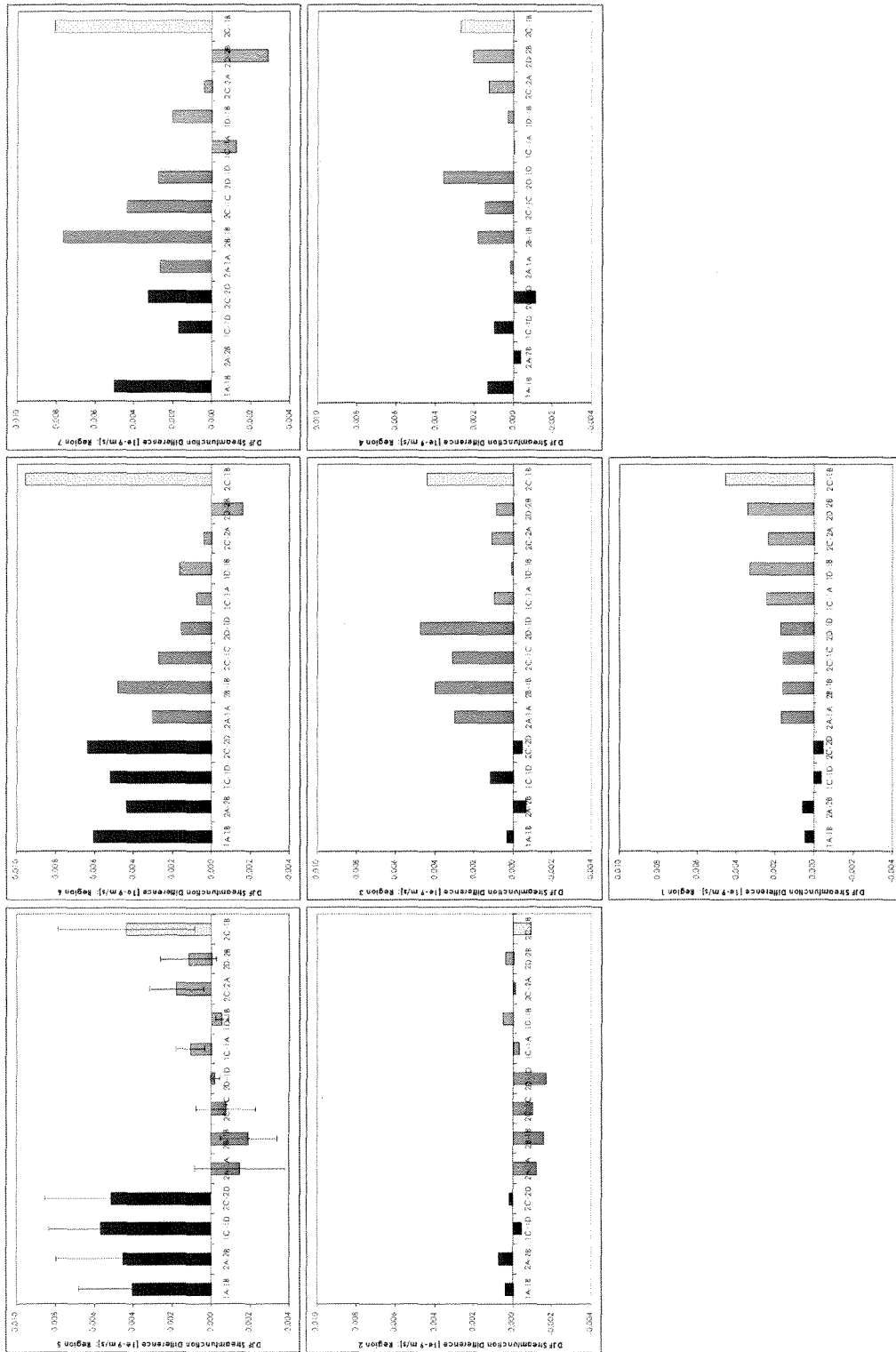


785 b)

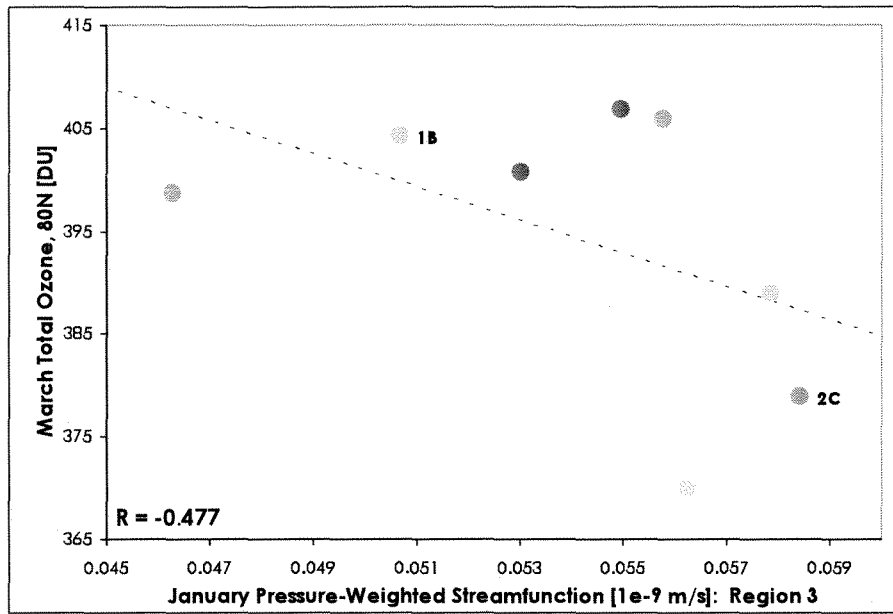
786

787 **Figure 5:** (a) Latitude–height cross–section showing the mean streamfunction for
788 experiment 1B, for the DJF season [1×10^{-9} kg/s³]. (b) Latitude–height cross–

789 section of the mean pressure-weighted streamfunction (the streamfunction
790 divided by the pressure in hPa) for experiment 1B for the DJF season [1×10^{-9} m/s].
791 The seven numbered boxes identify the atmospheric regions defined in section
792 5.1 of the text.



794 **Figure 6:** Pressure-weighted streamfunction differences between pairs of
795 experiments, for seven atmospheric regions, for the DJF season. The spatial
796 organization of the regions is as shown in figure 6b. The four bars for each set of
797 differences denote the DJF, MAM, JJA and SON seasons, respectively. The blue
798 bars represent the response to ozone recovery; the pink bars represent the
799 response to doubled CO₂; the green bars represent the response to increased
800 SSTs; the yellow bars represent the response in the climate change signal (2C-
801 1B). Error bars in region 5 denote ± 1 standard deviation.
802



802

803 **Figure 7:** January streamfunction in region 3 versus March total column ozone at
804 80°N. The colored circles show the 20-year mean for each time-slice
805 experiment; the dashed line shows the line of best fit, fitting the eight mean
806 values.